# Study of Fe-doped $La_{1-x}Ca_xMnO_3$ ($x \simeq 1/3$) using Mössbauer spectroscopy and neutron diffraction

A. Simopoulos, M. Pissas, G. Kallias, E. Devlin, N. Moutis, I. Panagiotopoulos, D. Niarchos, and C. Christides
*Institute of Materials Science, National Center for Scientific Research ''Demokritos,'' 153 10 Aghia Paraskevi, Athens, Greece*

R. Sonntag
*Berlin Neutron Scattering Center, Hahn-Meitner-Institut Glienicker Strasse, 100 D-14109 Berlin, Germany*
(Received 3 June 1998)

$La_{2/3}Ca_{1/3}MnO_3$ doped with Fe were studied by Mössbauer spectroscopy and neutron powder diffraction. The Mössbauer spectra (MS) reveal that Fe substitutes for Mn as $Fe^{3+}$ ($S=5/2$) and is antiferromagnetically coupled to the Mn host lattice. The magnetic behavior, from the neutron diffraction data, is that of a typical 3D Heisenberg ferromagnet. The temperature evolution of the MS differs from that of the neutron data, especially above 40 K. The data can be interpreted using a model based on an antiferromagnetic impurity in a ferromagnetic host. In such a system, the ground state is inhomogeneous resulting in spin states with reduced spin and the spin excitations are localized in the immediate neighborhood of the impurity atoms. Finally, at $T \approx 0.9T_c$ the MS indicate the onset of charge localization. [S0163-1829(99)09101-8]

## I. INTRODUCTION

The discovery of ''colossal'' magnetoresistance (CMR) in oxide films of the perovskite $La_{0.67}Ca_{0.33}MnO_3$ class of compounds by Jin *et al.*[1] has recently attracted significant scientific attention. This effect appears at a temperature where the system undergoes a metal-insulator transition associated with the simultaneous appearance of ferromagnetic order. The physics of this phenomenon so far has been focused on the double exchange (DE) of carriers between the $Mn^{3+}$ and $Mn^{4+}$ ions, the latter being created to balance the charge deficit from the divalent $Ca^{2+}$ doping.[2] Millis *et al.*[3] have suggested that DE alone cannot explain the dramatic change of the resistivity and they have shown that electron-phonon coupling arising from the Jahn-Teller distortion of the $Mn^{3+}$ ion is also necessary for the CMR effect.

Numerous investigations in this field indicate that the magnetic transition is not a conventional second order transition. Neutron scattering studies[4] in the $x=1/3$ compound have shown a quasielastic magnetic component which becomes dominant at temperatures close to $T_c$. This component has been associated with electron localization on a short length scale. Among the possible mechanisms for charge localization is that of lattice distortions.[3] Unusual spin relaxation dynamics were observed in the same system by muon spin relaxation measurements[5] and were interpreted as arising from variable-size spin clusters below $T_c$.

Ahn *et al.*[6] studied the influence of iron doping $y$ in the $La_{1-x}Ca_xMn_{1-y}Fe_yO_3$ ($y \geqslant 0.08$) compound. The similar ionic radii of $Fe^{3+}$ and $Mn^{3+}$ mean that lattice distortion effects of the substitution may be ignored, and the electronic structure can be studied. Using a simple energy band diagram they have shown that only the Mn $e_g(up)$ band is electronically active, where electron hopping between the $Mn^{3+}$ and $Mn^{4+}$ occurs. The Fe $e_g(up)$ band is completely filled and electron hopping from $Mn^{3+}$ to $Fe^{3+}$ is forbidden. Since $Fe^{3+}$ replaces $Mn^{3+}$, doping with Fe reduces the $Mn^{3+}/Mn^{4+}$ ratio, and reduces the number of available hopping sites. Thus DE is suppressed, resulting in the reduction of ferromagnetic exchange, and metallic conduction.

The nonparticipation of iron in the double exchange may have consequences for Mössbauer experiments. As the iron does not share the same interactions as the manganese ions there is a question whether it can give an accurate picture of the $Mn^{3+}/Mn^{4+}$ host. In order to investigate further this problem we have studied the compound $La_{2/3}Ca_{1/3}MnO_3$ doped with 1% $^{57}Fe$. Preliminary results have been given in Refs. 7 and 8. Undoped, 1% and 2% Fe-doped samples were also studied by neutron diffraction for comparison. The data show that the Fe impurity is antiferromagnetically coupled to the ferromagnetic host. As such, it is a model system for theoretical investigations[9–14] of this special magnetic configuration. Theoretical predictions, and the experimental data on the temperature evolution of the spectra, indicate that magnetic excitations, localized at the impurity atoms, play an important role.

## II. EXPERIMENT

Two sets of iron-doped samples were prepared. The first set, used for Mössbauer measurements, contained 90% enriched $^{57}Fe$, and the second set, for neutron scattering studies, natural iron. Four powder samples with nominal composition $La_{1-x}Ca_xMn_{1-y}A_yO_3$, [($A=^{57}Fe$, $x=0.33$, $y=0.01$) $\equiv$FE1, ($x=0.34$, $y=0.0$)$\equiv$N0, ($A=$Fe, $x=0.34$, $y=0.01$) $\equiv$N1, ($A=$Fe, $x=0.34$, $y=0.02$)$\equiv$N2] were prepared by solid state reaction of stoichiometric amounts of $La_2O_3$, $CaCO_3$, $MnO_2$, and $Fe_2O_3$ at 1300 °C for 5 days with intermediate grindings and reformation into pellets each time. The x-ray powder diffraction data revealed single phase materials. The structural studies and the estimation of the lattice parameters were carried out using the Rietveld refinement method (assuming the orthorhombic *Pnma* space group). The bulk magnetic moment measurements were performed using a SQUID magnetometer (Quantum Design). The $T_c$ for the N0, N1, N2, and FE1 samples were estimated from magnetic measurements [inflexion point in the $M(T)$ curve] to be 267, 260, 250, and 228 K, respectively.

 

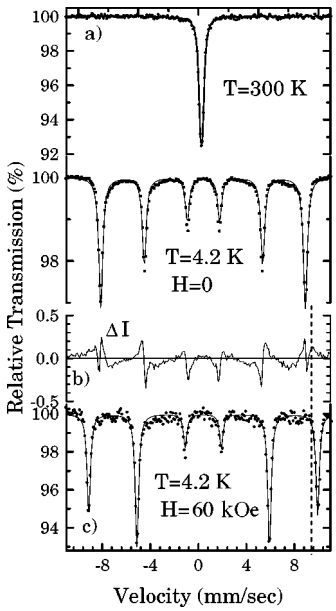


FIG. 1. Mössbauer spectra for the $La_{0.67}Ca_{33}Mn_{0.99}{}^{57}Fe_{0.01}O_3$ sample at (a) RT and 4.2 K, together with the difference between the experimental and the theoretical spectra (b) and (c) at 4.2 K in the presence of a 60 kOe magnetic field.

Absorption Mössbauer spectra (MS) were collected with a $^{57}$Co(Rh) source moving at room temperature (RT), while the absorbers were in a variable temperature cryostat equipped with a 65 kOe superconducting magnet, with the field perpendicular to the gamma-ray beam. The neutron powder diffraction (NPD) experiments were performed in the flat-cone diffractometer E2 of the research reactor BERII in Berlin. The (002) reflection of a pyrolytic graphite monochromator with wavelength $\lambda \simeq 2.4$ Å was used. The sample was loaded into a vanadium holder and placed in a cryostat for temperature dependence measurements.

## III. RESULTS AND DISCUSSION

### A. Mössbauer data

Figure 1(a) shows the MS of the FE1 sample at 300 and at 4.2 K in zero field. The $T=300$ K spectrum consists of a single absorption line which was fitted with a quadrupole doublet having isomer shift $\delta=0.368(2)$ mm/s with respect to $\alpha$-Fe at RT and quadrupole splitting $\Delta E_Q=2\varepsilon=0.184(3)$ mm/s. The isomer shift is typical of $Fe^{3+}$ ions in octahedral coordination, while the small quadrupole splitting indicates a slight distortion of the octahedron. The 4.2 K spectrum corroborates this result displaying a magnetic sextet with hyperfine parameters $H=531.5(1)$ kOe, $\delta=0.515(1)$ mm/s and $\varepsilon=-0.018(1)$ mm/s which are typical for high spin ($S=5/2$) trivalent Fe. From the value of $\varepsilon$ $[\varepsilon=e^2qQ(3\cos^2\theta-1)/4]$ an angle of $\approx 59°$ is determined between the $z$ axis of the electric field gradient (EFG) and the hyperfine magnetic field direction $H$.

The 4.2 K spectrum with $H_{\rm ext}=60$ kOe is shown in Fig. 1(c). The intensities of the absorption lines have changed from a 3:2:1 ratio at zero field to 3:4:1 showing that the magnetic moments have been oriented parallel to the applied magnetic field. The hyperfine field at the Fe nucleus has increased by 60 kOe indicating that the spin of the Fe ion orients antiparallel to the applied magnetic field, i.e., it is coupled antiferromagnetically to its Mn neighbors. This is due to the absence of the ferromagnetic DE interaction, i.e., the absence of electron hopping to the Fe site, as noted by Ahn *et al.*[6] Leung *et al.*[15] arrived at a similar conclusion in their studies of the $La_{1-x}Pb_xMn_{1-y}Fe_yO_3$ system with Fe doping ($0.03 \leqslant y \leqslant 0.17$). The hyperfine parameters at $T=300$ and 4.2 K obtained from the fitting procedure are summarized in Table I. Figure 1 also shows that at 4.2 K there is a small spectral area which is not fitted with the $H=531.5$ kOe magnetic sextet, indicating iron sites with an average hyperfine field smaller than the saturation value of the majority of the Fe nuclei.

TABLE I. Experimental values of the half linewidth $\Gamma/2$ in mm/s, the isomer shift $\delta$ relative to metallic Fe at RT in mm/s, $\varepsilon$ in mm/s, the hyperfine magnetic field $H$ in kOe, as obtained from least squares fits of the Mössbauer spectra of the $La_{0.67}Ca_{0.33}Mn_{0.99}Fe_{0.01}O_3$ sample. $\varepsilon$ denotes the eigenvalues of the Hamiltonian of the quadrupole interaction or of the quadrupole perturbation that are given by the relations $\varepsilon=(1/4)e^2qQ(1+\eta^2/3)^{1/2}$ and $\varepsilon=(1/8)e^2qQ(3\cos^2\theta-1+\eta\sin^2\theta\cos 2\phi)$ for the paramagnetic and the magnetic case, respectively. The numbers in parentheses are estimated standard deviations referring to the last significant digit. $(*)H_{\rm ext}=60$ kOe. $(+)$ $\varepsilon\simeq 0$ due to its integration over the surface of a sphere.

| $T$ (K) | $\delta$ | $\varepsilon$ | $\Gamma/2$ | $H$ | $\theta$ |
|---|---|---|---|---|---|
| 300 | 0.368(2) | 0.092(3) | 0.174(1) | | |
| 4.2 | 0.515(1) | −0.018(1) | 0.172(2) | 531(1) | 59° |
| 4.2* | 0.510(2) | $-0.000(2)^+$ | 0.171(2) | 594(1) | |

Figure 2 shows the MS taken at temperatures between 4.2 K and the transition temperature $T_c^M$—the temperature where the MS is completely paramagnetic—for the FE1 sample. The temperature $T_c^M=228$ K coincides with the critical temperature determined by magnetization measurements. The spectra display an asymmetric line broadening at relatively low temperatures ($\approx$40 K) which increases further as the temperature increase. At temperatures above 78 K the two central lines protrude with an increasing tendency, and at about 210 K they collapse to a broad single line, which narrows and dominates the spectrum as we approach $T_c$. This is distinctly different to the temperature evolution of the MS of the $La_{0.75}Ca_{0.25}Mn_{0.98}Fe_{0.02}O_3$ sample,[7] where the asymmetric broadening is not as pronounced, and at 78 K the spectrum shows two small peaks between lines 3 and 4, and as the temperature increases these peaks merge and give a paramagnetic unresolved doublet. It should be noted that line broadening of the Mössbauer spectra at elevated temperature has been observed in all the studies reported so far for Fe-doped La manganites.[15–17]

Mössbauer spectroscopy, in the ferromagnetic state, measures the hyperfine field $H_{\rm eff}(T)$ (via the line splitting) which probes the spontaneous magnetization $M(T)$ of the ferromagnetic phase at the iron sites. For a typical isotropic ferromagnet, such as $\alpha$-Fe, the MS below the critical temperature consist of a sextet with narrow Lorentzian lines. As the temperature increases from zero, the Zeeman splitting de-

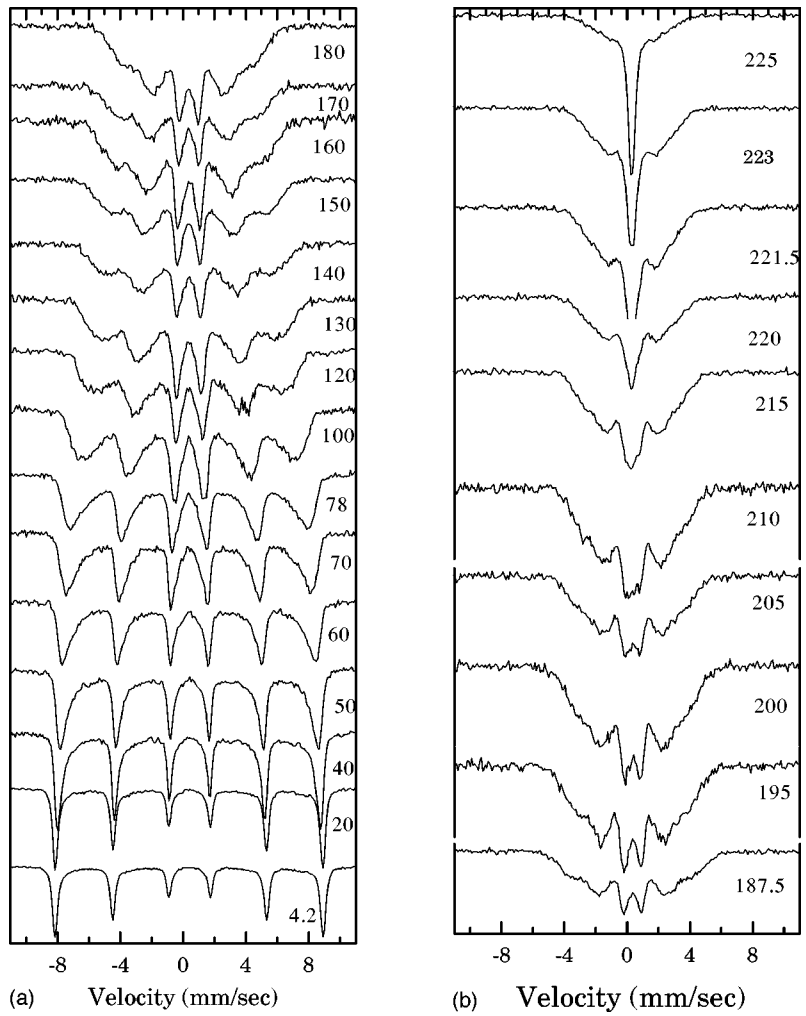


FIG. 2. Mössbauer spectra from 4.2 K to 180 K (a) and from 187.5 up to 225 K (b) for the $La_{0.67}Ca_{33}Mn_{0.99}{}^{57}Fe_{0.01}O_3$ sample.

creases while the line width remains constant up to the critical regime. Line broadening due to collective excitations (spin waves) is unobserved because the fluctuations of **S** with respect to $\langle \mathbf{S} \rangle$, in such a case are so fast (in comparison with a Larmor frequency at a field of 200 kOe $f_L = 5 \times 10^9$ Hz) that they average out. This is true in normal ferromagnets where the bottom of the spin wave branch is higher than the Mössbauer frequencies (except in the immediate vicinity of $T_c$ where very small critical effects have been observed). Based on the above discussion and the experimental results the MS for FE1 sample do not display the behavior expected for a typical ferromagnet.

Line broadening (in magnetically ordered systems) of MS may be due to several reasons. The most common are chemical inhomogeneities (macroscopic and/or microscopic), superparamagnetic behavior due to small crystallite size, relaxation of spin clusters, spin glass behavior, and local environment effects. The case for inhomogeneities is neither supported by the well defined 300 and 4.2 K spectra, nor by the coincidence of the $T_c$ with $T_c^M$. Similarly, in the case of amorphous or spin glass magnetic systems we would expect to observe broad magnetic MS for $T < T_c$, present down to low temperatures ($T/T_c \rightarrow 0$), in contrast with the present MS. Paramagnetic relaxation is also excluded by elastic neutron diffraction studies and bulk magnetization measurements on these samples which show long range order and ferromagnetic behavior. Exclusion of the above leaves us with local environment effects. A model based on an impurity that is antiferromagnetically coupled to a ferromagnetic host, predicts low lying spin states which can reproduce the spectra observed. In the following a detailed analysis of the MS is undertaken.

At 4.2 K the MS display an intense (90%) well-defined component and a weaker ($\sim$10%) broad spectral feature which corresponds to smaller effective hyperfine magnetic fields [see Fig. 1(b)]. There are two possible interpretations for these features. The simpler explanation is to attribute them to iron atoms with $n$ iron atoms as nearest neighbors. The assumption is that the hyperfine field at a given Fe site is reduced (or increased) by an amount proportional to the number of Mn nearest neighbors and next near neighbors. Supposing that the iron ions are homogeneously distributed at the Mn sites, the probability for the iron ion to have $n$ ($n = 1,2, \ldots ,6$) iron ions as nearest neighbors is given by the binomial distribution, $P(n,y) = [6!/(n!(6-n)!)]y^n(1-y)^{6-n}$, where $y$ is the percentage of iron in a formula unit. In our case we have $P(0,1\%) \simeq 94.1\%$, $P(1,1\%) \simeq 5.7\%$, and $P(2,1\%) \simeq 0.2\%$ for $y = 1\%$ iron doping. The experimental spectrum area which does not belong to the sharp sextet is estimated to be $\simeq$10% of the overall spectrum area

and could be attributed to Fe sites with one or two nearest neighbor iron ions. Although it is attractive to attribute the small spectral area to configurations where iron has as first nearest neighbor one or two iron ions, such a distribution would be temperature independent. In our spectra however, the spectral area which is small at 4.2 K increases and becomes comparable in intensity with the major sextet at about 100 K. Furthermore, the replacement of a Mn nearest neighbor with Fe is expected to result in larger local hyperfine fields, not as observed in this material.

A second interpretation of the weaker, broad spectrum component is that it is due to occupation by the iron of another spin state. This spin state represents a small degree of zero point oscillation of the iron moment. Such low lying spin states for the iron are created in systems such as this where an ion is weakly coupled to its neighbors. This possibility has been described thoroughly by Izyumov (Ref. 9). In the Appendix we give a short description of that theory as it applies to the present situation. Here we note just that the zero point oscillation disturbs the first neighbors and as a result the host atoms near the impurity have reduced spin projections even in the ground state, producing thus a smaller hyperfine field. Thus there exist localized excitations, i.e., states where the reduction of the total spin is localized in the vicinity of the impurity. An increase of this part of the spectrum going from 40 up to 100 K is associated with the thermal population of such states, representing different magnitudes of the impurity spin, and as a consequence a broad distribution of $H_{\text{eff}}$. Above 120 K complex configurations are occupied.

Following this theory, we modeled the MS with a discrete distribution of $H_{\text{eff}}$ as a sum of sextets with Lorentzian line shape with the same line width, isomer shift, and quadrupole interaction. Figure 3 shows the resulting fit of the MS for FE1 at 4.2, 50, 150, and 223 K using the discrete distribution model. The effective hyperfine magnetic field distributions extracted at each temperature are shown is Fig. 4. Figure 5 displays the variation of the most probable effective hyperfine magnetic field with temperature. Also plotted are the upper and lower interval of $H_{\text{eff}}$ where $p(H_{\text{eff}})$ is different from zero, and the ordered magnetic moment per ion as it is estimated from neutron data. The most probable value of $p(H_{\text{eff}})$, which represent the majority of Fe atoms, does not follow the average ordered moment. The same holds for the upper limit of $H_{\text{eff}}$. The $H_{\text{eff}}$ starts to decrease appreciably around 40 K. Similar behavior is observed in $La_{0.75}Ca_{0.25}Mn_{0.98}Fe_{0.02}O_3$, although the reduction is slower.[7] In both samples $H_{\text{eff}}$ falls below the variation of the magnetic moment of the host as a function of the temperature as observed by neutron diffraction measurements.

Clearly, at low temperature the iron spin has the maximum value (the spin deviation of the iron is small) and as the temperature increases the localized states where ($S=3/2$ and $S=1/2$) are thermally populated. As the temperature increases further the distribution becomes broad. This unusual variation of the magnetic hyperfine field has been observed by Tkatchuk *et al.* in $La_{0.83}Sr_{0.17}Mn_{0.98}Fe_{0.02}O_3$ and was accounted for using a simple model proposed by Jaccarino *et al.*,[18] in agreement with the present treatment.

A third (paramagnetic) component is necessary to fit the spectra at and above 200 K. The hyperfine parameters of this component are the same as those observed above $T_c$. The intensity of this component increases with temperature at the expense of the intensities of the magnetic components. Similar behavior was observed in $^{119}$Sn Mössbauer measurements in a 5% Sn doped sample.[8] This result corroborates the conclusion of Lynn *et al.*[4] from the neutron data about the existence of a high temperature paramagnetic phase.

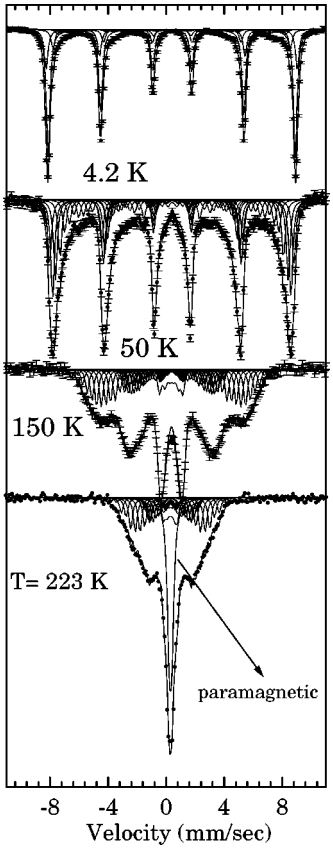


FIG. 3. Fit of the Mössbauer spectra for $La_{0.67}Ca_{33}Mn_{0.99}{}^{57}Fe_{0.01}O_3$ sample at 4.2, 50, 150, and 223 K using a discrete distribution of hyperfine magnetic fields. All the subcomponents have the same line width, isomer shift, and quadrupole interaction.

The MS in the vicinity of $T_c$ in a 60 kOe applied magnetic field are shown in Fig. 6. At $T>T_c$ the external magnetic field produces a broad magnetic MS in the place of the paramagnetic doublet. Similarly the external magnetic field significantly reduces the paramagnetic component of the MS for $T\simeq T_c$ and $T<T_c$. The MS show the same phenomenon near $T_c$ as neutron inelastic scattering studies where the quasielastic component is associated with electron localization on a short length scale. If the itinerant electrons are localized, the system cannot gain energy from ferromagnetic oriented spins. So the long range correlation of the magnetic moments tends to zero. It is worth mentioning that the particular behavior of the MS near $T_c$ is related to the first order nature of the transition, as indicated by NMR studies.[19]

A last remark should be made. The overall picture of the spectra (for $T>100$ K) is reminiscent of the superparamagnetic behavior with unequal magnetization direction probabilities.[20] We can reproduce the MS using the spin relaxation model developed by van der Woude and Dekker.[21] This model quite accurately reproduces the enhancement of

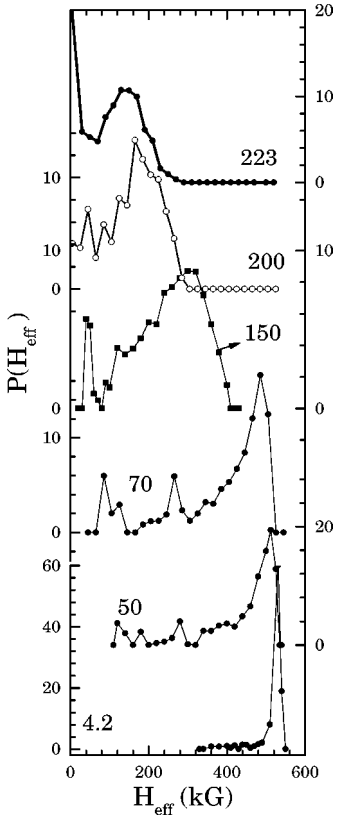


FIG. 4. Distribution of hyperfine magnetic fields for $La_{0.67}Ca_{33}Mn_{0.99}{}^{57}Fe_{0.01}O_3$ sample at 4.2, 50, 70, 150, 200, and 223 K as extracted from corresponding MS using a discrete distribution of hyperfine magnetic fields.

the two central lines of the spectra which appears in the intermediate temperature regime. In the fitting procedure the free parameters were the spin relaxation rate $\Omega$, the order parameter $\eta$, and the intensity of each of the two components, while the experimental linewidth $\Gamma$ and the hyperfine magnetic field $H$ were kept constant to the values determined from the ''static'' spectrum at 4.2 K. Two more parameters in the fitting program are the quadrupole interaction $\epsilon$, which is also kept constant at its 4.2 K value, and the isomer shift

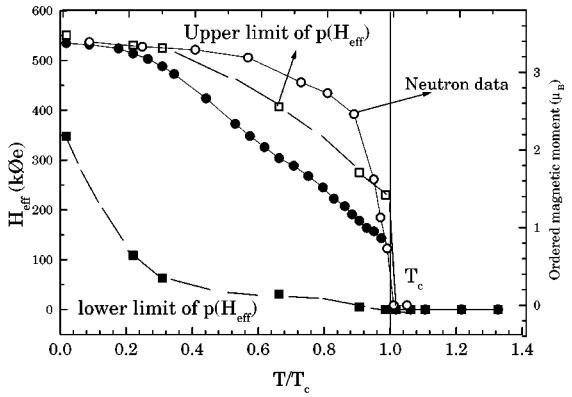


FIG. 5. Variation of the most probable effective hyperfine magnetic field (peak value of the distribution) (filled circles), upper limit of $H_{\rm eff}(T)$ (open squares), lower limit of $H_{\rm eff}(T)$ (filled squares) of the FE1 sample, and of the ordered magnetic moment per ion for the N1 sample (open circles) as a function of $T/T_c$.

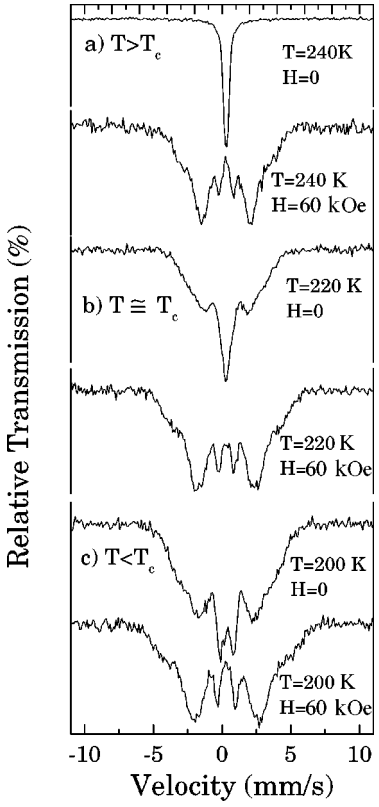


FIG. 6. Mössbauer spectra of the FE1 sample in zero and 60 kOe applied magnetic field (a) at $T > T_c$ (b), at $T \approx T_c$, and (c) at $T < T_c$.

which was kept constant at each temperature to the value deduced from its linear temperature relationship between 80 K and RT. The dynamic model reproduces accurately and consistently the MS although it does not agree with the magnetization and neutron diffraction data which indicate a 3D Heisenberg ferromagnet behavior. This contradiction may be due to the fact that the Fe probe, which does not participate in the double exchange mechanism of the Mn ions, does not follow the bulk magnetization of the system but rather witness the dynamic effects of its immediate environment. Such effects may be the localized excitations around the impurity or the charge fluctuations near the impurity, both being in a time scale comparable to the Mössbauer time window ($10^{-7}$–$10^{-8}$ sec). Near 200 K charge localization sets in resulting in a paramagnetic phase which spreads fast in the system as the temperature increases. An alternative description of the phenomena observed above 200 K is that this ''paramagnetic'' phase is the result of regions with fast relaxing magnetic moments ($\Omega > 100$ Mc). Application of a magnetic field of 60 kOe at higher temperatures results in slowing down the spin fluctuation rates significantly. The paramagnetic component has disappeared in agreement with the neutron inelastic scattering data.[4]

### B. Neutron diffraction data

The diffraction patterns were refined by Rietveld profile analysis using the FULLPROF program,[22] with the peak shapes approximated by a pseudo-Voigt function. The results of the refinement above $T_c$ and at low temperatures are listed in Table II. The fitted neutron diffraction patterns for $y = 0$, 1,

TABLE II. Refined fractional atomic positions, average Debye-Waller factors, unit cell parameters, Mn site magnetic moment and reliability factors derived from neutron diffraction data for the $La_{1-x}Ca_xMn_{1-y}Fe_yO_3$ ($y=0$, 0.01, 0.02) samples measured with $\lambda=2.397$ Å. The space group $Pnma$ (No. 62) was used. La, Ca, and O(1) occupy the $4c$, ($x$, 1/4, $z$) sites, Mn the $4b$ ($x$, 0, 1/2) site and O(2) the general $8d$ site. The numbers in parentheses are estimated standard deviations referring to the last significant digit.

| | $y=0.0$ | $y=0.01$ | | $y=0.02$ | |
|---|---|---|---|---|---|
| $T$ (K) | 275 | 2 | 280 | 20 | 260 |
| $a$ (Å) | 5.464(2) | 5.450(1) | 5.460(2) | 5.452(2) | 5.459(2) |
| $b$ (Å) | 7.716(2) | 7.697(2) | 7.711(2) | 7.691(2) | 7.703(2) |
| $c$ (Å) | 5.473(2) | 5.461(2) | 5.463(3) | 5.454(2) | 5.465(3) |
| La $x$ | 0.024(1) | 0.0229(9) | 0.025(9) | 0.024(1) | 0.026(1) |
| $z$ | −0.009(2) | −0.011(2) | −0.001(3) | −0.011(3) | −0.010(3) |
| $B$ (Å$^2$) | 0.9 | 0.3(1) | 0.9(1) | 0.3(1) | 0.8(1) |
| Mn $B$ (Å$^2$) | 0.9 | 0.2(1) | 0.6(1) | 0.2(1) | 0.5(1) |
| O(1) $x$ | 0.488(1) | 0.491(2) | 0.489(2) | 0.491(2) | 0.490(2)) |
| $z$ | 0.062(2) | 0.063(2) | 0.069(4) | 0.063(2) | −0.067(3) |
| $B$ (Å$^2$) | 1.3 | 0.8(2) | 1.5(1) | 0.8(1) | 1.4(1) |
| O(2) $x$ | −0.275(2) | −0.275(2) | −0.275(1) | −0.273(3) | −0.277(2) |
| $y$ | −0.032(1) | −0.033(1) | −0.029(2) | 0.033(1) | −0.032(1) |
| $z$ | 0.277(2) | 0.276(1) | −0.275(3) | 0.279(2) | 0.276(2) |
| $B$ (Å$^2$) | 1.6 | 0.9(1) | 1.5(1) | 0.9(1) | 1.4(2) |
| $S$ ($\mu_B$) | 0 | 3.45(5) | 0.00(6) | 3.39(3) | 0.02 |
| $R_{wp}$ | 6.6 | 13.1 | 10.20 | 8.7 | 9.33 |

and 2 % iron doping at $T=200$, 210, and 200 K, respectively, are shown in Fig. 7. Figure 8 displays the fitted neutron diffraction pattern for $y=1\%$ sample at 2 K. The crystal structure refinement was based on the space group $Pnma$ using as initial parameters these of XRD data. Except from the crystal structure parameters we included in the refinement the scale factor, the zero angle, and the $n$-mixing parameter for the Lorentzian and Gaussian components in the pseudo-Voigt function. Since the monitor (total number of counts collected at each temperature) is known, by assuming that near $T\sim 0$ K the temperature factors are close to zero an estimation of the scale factor was done at 2 K. Correcting this scale factor for the unit cell expansion with temperature we left the $B$ factors as free parameters while keeping the scale factor constant. This method gives a reliable estimation of $B_i$ and of the ordered magnetic moment. In addition to the crystal structure model we include a magnetic structure model based on ferromagnetic interactions between nearest neighbor manganite ions. From the magnetic structure model we estimated the amplitude of the ordered magnetic moment per manganese ion as a function of temperature. The variation of ordered magnetic moment for all the samples is plotted in Fig. 9. As the iron doping level increases the $T_c$ systematically decreases and a broadening of the transition for the $x=2\%$ sample is clearly observed. The static critical behavior of the order parameter (spontaneous magnetization) $M(T)$ of a magnetic system is characterized by the critical exponent $\beta$ which is defined by the asymptotic relation $M(T)/M(0)=B(1-T/T_c)^{\beta}$, $T\rightarrow T_c$ (or $t=1-T/T_c$

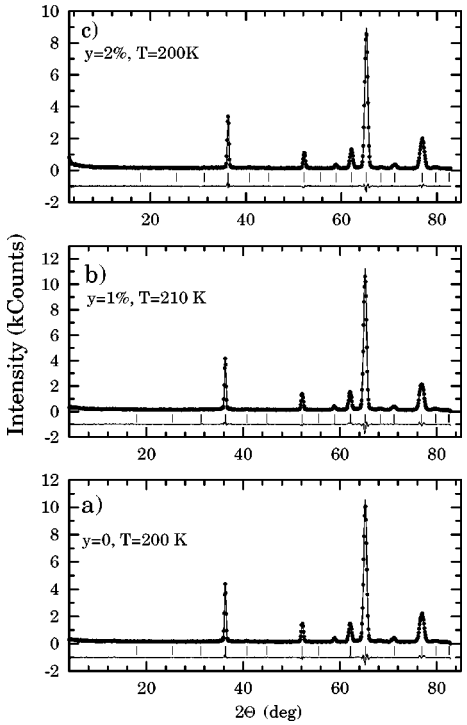


FIG. 7. Rietveld refinement plots of the neutron powder diffraction data obtained with $\lambda=2.397$ Å at the indicated temperatures for the samples $La_{0.36}Ca_{0.34}Mn_{1-y}Fe_yO_3$: (a) $y=0$, (b) $y=0.01$, and (c) $y=0.02$. The solid line is the calculated profile and the bars below denote the allowed Bragg reflection positions. The difference between the experimental and theoretical fits is also plotted.

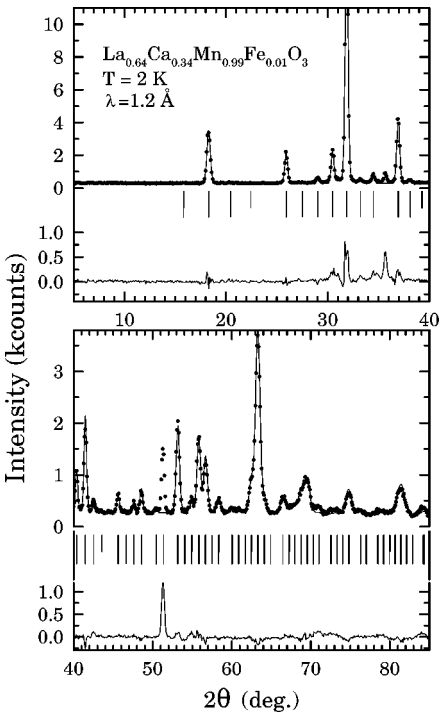


FIG. 8. Rietveld refinement plot of the neutron powder diffraction data obtained with $\lambda = 1.217$ Å at 2 K for the $La_{0.66}Ca_{0.34}Mn_{0.99}Fe_{0.01}O_3$ sample (N1). The solid line is the calculated profile and the bars below denote the allowed Bragg reflection positions. The difference between the experimental and theoretical fits is also plotted. The excluded regions between 35–37° and 50.5–52.5° correspond to peaks due to the cryostat.

$<10^{-2}$). For temperatures not sufficiently close to $T_c$ the asymptotic relation must be modified with a correction-to-scaling term[23]

$$M(T)/M(0) = Bt^{\beta}[1 + At^{\beta_1} + O(t^{2\beta_1})], \qquad (1)$$

where $A$ is the correction-to-scaling amplitude and $\beta_1$ is the correction-to-scaling exponent. For static universality class ($D=3$, $n=3$), holds[23] $\beta = 0.365$, and $\beta_1 = 0.550$. Using Eq. (1) we estimated the parameters $\beta$, $A$, and $\beta_1$ via least square fitting of the neutron data for $y=0$, 1 and 2% samples. The

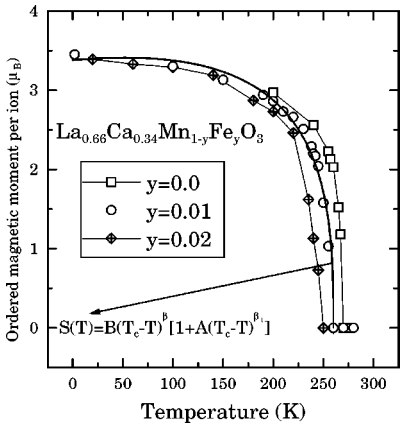


FIG. 9. Temperature dependence of the ordered magnetic moment per ion derived from neutron diffraction measurements for the samples $La_{0.66}Ca_{0.34}Mn_{1-y}Fe_yO_3$: (a) $y=0$, (b) $y=0.01$, and (c) $y=0.02$.

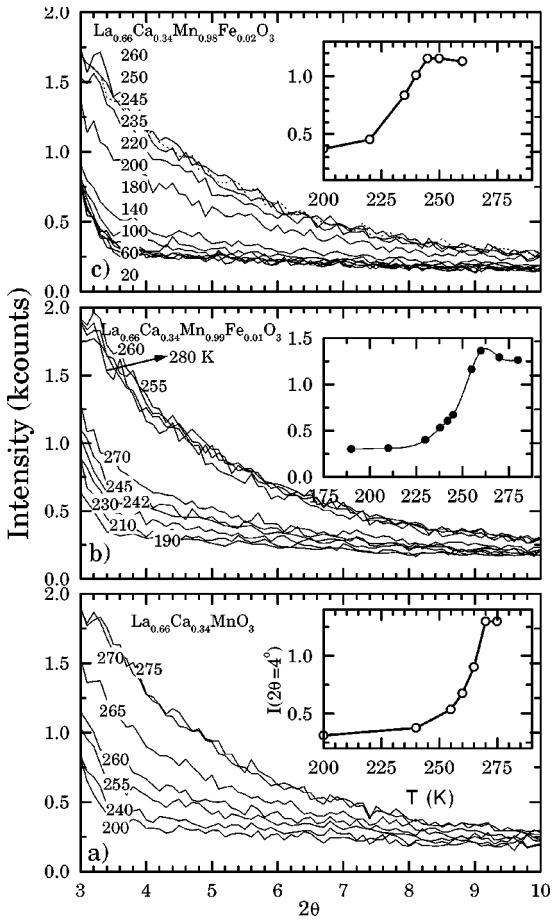


FIG. 10. Neutron diffraction patterns in the small $2\theta$ region for samples $La_{0.66}Ca_{0.34}Mn_{1-y}Fe_yO_3$: (a) $y=0$, (b) $y=0.01$, and (c) $y=0.02$. The insets in the three panels are the scattered intensity, at an angle of $2\theta = 4°$, as a function of temperature, indicating the existence of magnetic incoherent scattering around the transition temperature.

parameters for $y=1\%$ are $T_c \simeq 260$ K, $B = 0.78 \pm 0.07$, $\beta = 0.38 \pm 0.01$, $\beta_1 = 0.4 \pm 0.1$ and $A = -0.03 \pm 0.01$. These parameters are close to those predicted from the universality class of 3D Heisenberg Hamiltonian. At this point we must note that due to the limited number of data points the above parameters must be considered as indicative.

Figure 10 shows the temperature dependence of the small angle part of the diffraction pattern, which consists of the small angle intensity, the background and the incoherent nuclear contribution. The insets in Fig. 10 show the intensity at $2\theta = 4°$ as a function of temperature. For a simple ferromagnet as we cross $T_c$ we expect a divergence of the small angle intensity due to the critical fluctuations, while below $T_c$ the small angle intensity tends to zero. In our data the intensity does not go abruptly to zero below $T_c$, but within 25 K for $x=0$ sample and in larger intervals for $x=1\%$ and 2%. In addition, above the peak which coincides with $T_c$, a plateau is shown in agreement with the measurements of Teresa *et al.*[24,25]

A fitting of small angle intensity with a Lorentzian-type $q$ dependence $[I = I_0/(q^2 + (1/\xi)^2)]$ where $\xi$ is the magnetic correlation length gives for $T > T_c$, $\xi \cong 15$ Å for the $y = 0.01$ sample. The presence of non-negligible small-angle intensity above and below $T_c$ probably implies the presence

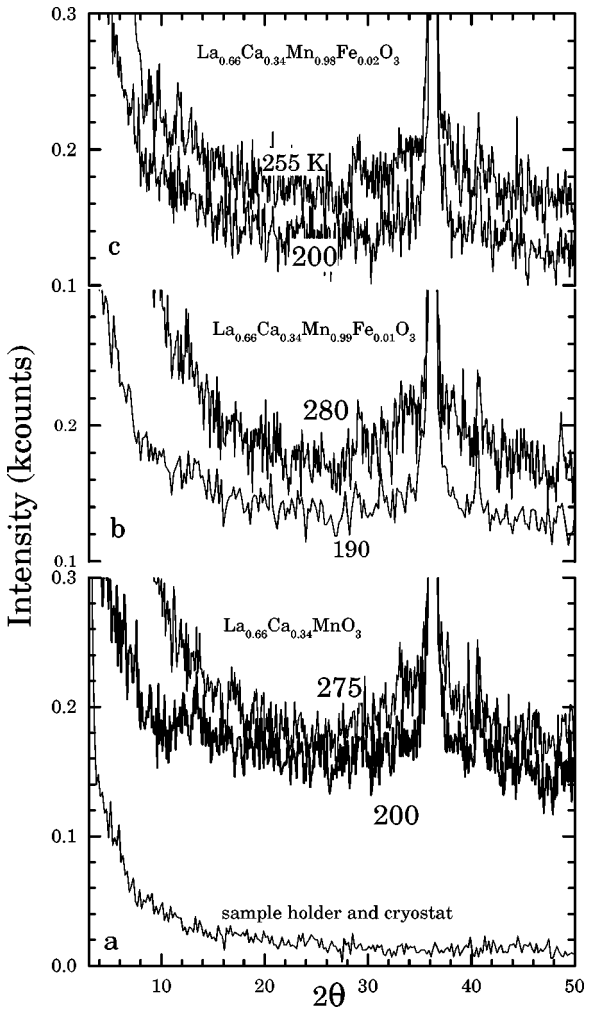


FIG. 11. Neutron diffraction patterns at the bottom of the largest magnetic peak at temperatures just above and far below $T_c$ for samples $La_{0.66}Ca_{0.34}Mn_{1-y}Fe_yO_3$: (a) $y=0$, (b) $y=0.01$, and (c) $y=0.02$. The contribution from the sample holder and the cryostat, for the same monitor, is also shown in panel (a).

of magnetic clusters in this temperature region, in agreement with the MS data. Finally, in Fig. 11 we show the presence of diffuse scattering intensity at the region of the strongest magnetic peak at the $T_c$ for the three samples. This diffuse scattering intensity is reduced as temperature decreases and disappears only below 100 K. We can speculate that the diffuse intensity increases as the iron doping increases for the $T/T_c$ ratio. The existence of diffuse intensity may be originated from inhomogeneities or it is a fingerprint of magnetic clusters for $T<T_c$.

## IV. CONCLUSION

It is shown that the Fe moment is antiferromagnetically coupled to the ferromagnetic Mn host. The Fe substitutes for Mn as $Fe^{3+}$ $(S=5/2)$. The variation of $H_{\text{eff}}$ with temperature differs markedly from the temperature dependence of the average ordered magnetic moment per ion deduced from the neutron data, which is that of a typical 3D Heisenberg ferromagnet. The temperature variation of the magnetization correlates with the neutron data. Thus, we use a theoretical model based on an antiferromagnetic impurity in a ferromagnetic host which predicts the existence of localized excitations, increasingly populated with temperature, and manifested in the Mössbauer spectra as a broad distribution of the effective magnetic hyperfine field. Near $T_c$ charge localization comes into play as it is revealed from the presence of a paramagnetic or fast relaxing component in the MS. The neutron diffraction data for the iron doped samples are similar to those of the undoped compound.

## ACKNOWLEDGMENTS

We are grateful to Dr. G. Papavassiliou, Dr. K. Papatriantafilou, and Professor S. Lovesey for helpful discussions. Partial support for this work was provided by the E.C. through the CHRX-CT93-0116, Human Capital and Mobility Program (access to large-scale facilities) projects.

## APPENDIX: ANTIFERROMAGNETICALLY COUPLED IMPURITY IN A FERROMAGNETIC HOST

At low temperatures iron is mainly in $Fe^{3+}$ $S=5/2$ state and is coupled antiferromagnetically with the ferromagnetic mixed valence host. We summarize below the important results of the relevant theory as it was presented in the past by Izyumov and Medvedev in Ref. 9. The exchange Hamiltonian describing the system is

$$H=-J/2\sum_{\mathbf{L}\neq\mathbf{0}}\ \sum_{\mathbf{L}+\mathbf{L}_0\neq\mathbf{0}}\mathbf{S}(\mathbf{L})\cdot\mathbf{S}(\mathbf{L}+\mathbf{L}_0)$$

$$+|\mathbf{J}'|\sum_{\mathbf{L}_0}\mathbf{S}(\mathbf{0})\cdot S(\mathbf{L}_0). \tag{A1}$$

The sum over $\mathbf{L}$ means a sum over all the crystal and the sum over $\mathbf{L}_0$ is a sum over the six vectors which connect the impurity atom with its six nearest neighbors. In the classical approach in which the spin vectors $\mathbf{S}(\mathbf{L})$ are regarded as classical numbers, the energy minimum of the energy corresponds to a state in which the spin of the impurity atom is aligned antiparallel to the completely ordered spins of the host crystal. The $z$ projection of the total spin of the system will be $S^0=(N-1)S-S'$, for a lattice with $N$ sites. The quantum mechanical determination of the ground state (and exited states also) of the system described by the Hamiltonian of Eq. (A1) is a very difficult problem. Since the total spin of the system commutes with the exchange Hamiltonian the eigenergies should be labeled by the $z$ projections of the total spin $S^0$. The spectrum of the possible values $\hat{S}_z=\Sigma_i\hat{S}_i^z$ are: $S^0_{\max}=(N-1)S+S'$, $S^0_{\max}-1$, $S^0_{\max}-2,\ldots$. When $J'>0$ the ground state is this with maximum eigenvalue of the $\hat{S}_z$, namely the $S^0_{\max}$. If $J'<0$ we must calculate the energy of the system in states with different $z$ projections of the total spin $S^0$ and select those with the lowest energy. The wave functions of the system in question corresponding to the states with the $z$ projections of the total spin $S^0_{\max}$, $S^0_{\max}-1$, $S^0_{\max}-2,\ldots$ will be denoted by $\Psi_0,\Psi_1,\Psi_2,\ldots$, respectively, and the corresponding eigenenergies will be labeled as $E_0$, $E_1$, $E_2,\ldots$ .

Parkinson worked out[13] the most simpler case where $S'=1/2$ and $S=1/2$. In this case the ground state belongs into

the manifold of $\Psi_1$ states. In the weak coupling limit ($J'/J \rightarrow -0$) the ground state is the pure Nèel state ($\langle \Psi_1 | S_n^z | \Psi_1 \rangle = 1/2$ for $n \neq 0$ and $-1/2$ for $n=0$). In the strong coupling limit ($J'/J \rightarrow -\infty$) the spin at the impurity site differs greatly from $-1/2$ and the reduction of the spin in the nearest neighbor host sites differs significantly from zero ($\langle \Psi_1 | S_n^z | \Psi_1 \rangle = 0.476$ for $n \neq 0$ and $-0.36$ for $n=0$). We must note that the reduction of the host spin is not confined only at the nearest neighbor but in all the crystal, with a magnitude which decreases exponentially with distance from the impurity. In the case of an arbitrary impurity spin $S'$ the ground state of the system should be sought in the spectrum of many-particle deviations from the state $\Psi_0$ characterized by exactly parallel spins. Problems of this kind are very difficult to solve. However, when the ground state of a crystal for $J' < 0$ is close to the Néel state (or $|J'|/J \rightarrow 0$) the corrections can be found by the spin-wave method in which the operators of the spin deviations from the Néel state are introduced. We shall assume that the true ground state of the quantum Hamiltonian has the same value of the $z$ projection of the total spin. However since zero-point oscillations appear unavoidably in a system with oppositely oriented spins and since these oscillations result in a reduction of the spins (more accurately in a reduction of their projections onto the direction of the spontaneous moment) the ground state should be *inhomogeneous.* This is due to the fact that the $z$ projection of the total spin of the system is conserved because its operator commutes with the exchange Hamiltonian. Therefore, if the projection of the impurity spin becomes shorter under the influence of the exchange interaction this shortening should be compensated by the reduction in the projections of the spins in the host crystal (the $S_z = \Sigma_i S_i$ is a conserved quantity). Hence, when $N \rightarrow \infty$ the ground state of the system should be inhomogeneous.

For $J' < 0$ the theory arrives to the following conclusions relevant to the present results: (a) The ground state of the system is inhomogeneous resulting in spin states with reduced spin. (b) There are spin excitations which are localized at the impurity atom and its immediate environment. Some of these excitations can reduce the spontaneous moment by unity and they are located within the quasicontinuous excitation band (i.e., they are low-lying in energy).


[1] S. Jin *et al.*, Science **264**, 413 (1994).
[2] C. Zener, Phys. Rev. **82**, 403 (1951).
[3] A. J. Millis, P. B. Littlewood, and B. I. Shraiman, Phys. Rev. Lett. **74**, 5144 (1995).
[4] J. W. Lynn *et al.*, Phys. Rev. Lett. **76**, 4046 (1996); J. W. Lynn *et al.*, J. Appl. Phys. **81**, 5488 (1997); L. Vasiliu-Doloc *et al.*, *ibid.* **81**, 5491 (1997).
[5] R. H. Heffner *et al.*, Phys. Rev. Lett. **77**, 1869 (1996).
[6] K. H. Ahn *et al.*, Phys. Rev. B **54**, 15 299 (1996).
[7] M. Pissas *et al.*, J. Appl. Phys. **81**, 8 (1997).
[8] A. Simopoulos *et al.*, J. Magn. Magn. Mater. **177**, 860 (1998).
[9] Yu. A. Izyumov and V. Medvedev (unpublished).
[10] H. Ishii, J. Kanamori, and T. Nakamura, Prog. Theor. Phys. **33**, 795 (1965).
[11] T. Wolfram and J. Callaway, Phys. Rev. **130**, 2207 (1963).
[12] D. Hone, H. Callen, and L. R. Walker, Phys. Rev. **144**, 283 (1966).
[13] J. B. Parkinson, Solid State Commun. **5**, 419 (1967).
[14] S. W. Lovesey, Proc. Phys. Soc. London **89**, 893 (1966).
[15] L. K. Leung, A. H. Morrish, and B. J. Evans, Phys. Rev. B **13**, 4069 (1976).
[16] S. B. Ogale *et al.*, Phys. Rev. B **57**, 7841 (1998).
[17] A. Tkachuk *et al.*, Phys. Rev. B **57**, 8509 (1998).
[18] V. Jaccarino *et al.*, Phys. Rev. Lett. **13**, 75 (1964).
[19] M. M. Savosta *et al.*, Phys. Rev. Lett. **79**, 4278 (1997).
[20] D. G. Rancourt and J. M. Daniels, Phys. Rev. B **29**, 2410 (1984).
[21] F. van der Woude and A. J. Dekker, Phys. Status Solidi **9**, 775 (1965).
[22] J. Rodriguez-Carvajal (unpublished); Physica B **192**, 55 (1993).
[23] J. C. Le Guillou and J. Zinn-Justin, Phys. Rev. Lett. **39**, 95 (1977).
[24] J. M. Teresa *et al.*, Nature (London) **386**, 256 (1997).
[25] J. M. De Teresa *et al.*, Phys. Rev. B **56**, 3317 (1997).